Gas-Phase Hydrolysis of $SOCl_2$ at 297 and 309 K: Implications for Its Atmospheric Fate

Timothy J. Johnson,* Robert S. Disselkamp, Yin-Fong Su, Robert J. Fellows, Michael L. Alexander, and Crystal J. Driver*

Pacific Northwest National Laboratory, P.O. Box 999, Richland, Washington 99352

Received: September 18, 2002; In Final Form: May 16, 2003

The gas-phase hydrolysis of thionyl chloride ($SOCl_2$) has been investigated at 297 and 309 K in a mixing chamber using FTIR spectroscopy. Reagent concentrations of ~80 ppmv $SOCl_2$ at relative humidities (RH) of 1−63% were studied at 309 K, while humidities of 1−85% were used in the 297 K studies, all at a total pressure of ~1 atm in synthetic air. In each experiment, an aliquot of $SOCl_2$(g) was rapidly introduced into a chamber at fixed RH, quickly reaching a maximum and then decreasing exponentially, as monitored by time-resolved infrared spectroscopy. The only observed reaction products were HCl(g) and SO_2(g), which were formed in a molar ratio of ~2:1. The $SOCl_2$ decay data are consistent with, but do not prove, the reaction being a gas-phase hydrolysis that is first order in both $SOCl_2$ and H_2O, with the RH-dependent decay data indirectly suggesting the first-order dependence on H_2O(g). The 297 K rate constant was measured as $(6.3 \pm 3.5) \times 10^{-21}$ cm^3/molecule-s. Confirming previous results, $SOCl_2$ absorbed only at $\lambda < 290$ nm, which suggests hydrolysis as the main loss mechanism in the troposphere at typical temperatures and humidities.

Introduction

Thionyl chloride ($SOCl_2$) is an industrial compound[1] whose estimated global production is in the tens of thousands of tons per year. It is an extremely powerful oxidant, and one of its primary uses is in converting alcohols and carboxylic acids into their corresponding chlorides.[2] It has also been investigated as a potential means to chlorinate silica for chromatography columns.[3] In the last quarter century, $SOCl_2$ has garnered importance due to its role in lithium batteries, known for their high energy densities and long shelf lives. In these batteries, the lithium metal is oxidized at the anode, while at the cathode the thionyl chloride is reduced to chloride ion (Cl^-) and sulfur dioxide (SO_2).[4,5] Due to the importance of Li/$SOCl_2$ batteries, the electrochemical reduction of $SOCl_2$ has been studied extensively.[6] For example, Kim and Park[7,8] have undertaken several electrochemical and spectroscopic studies of the reduction, including the effects of $SOCl_2$ aggregation in certain organic solvents. Thionyl chloride not only appears to aggregate with itself in solution, but also forms aggregates with other species. Using Raman spectroscopy, Mosier-Boss et al.[9] found that it formed aggregates with $AlCl_3$.

There are numerous spectroscopic studies involving $SOCl_2$. Asundi and Samuel first reported the visible−ultraviolet spectrum[10] of the gas-phase species, and Takacs et al.[11] quantified and improved these results. $SOCl_2$ does not absorb in the visible or near-infrared, only starting to absorb near 290 nm, rising rapidly between 250 and 280 nm, and then more slowly to ~190 nm. The fact that $SOCl_2$ is transparent between 300 and 2500 nm has led to its use as a "transparent medium", for example, in studies on halogens and interhalogens[12] as well as in the aprotic system $SOCl_2-GaCl_3-UO_2Cl_2$, whereby it was hoped that the luminescent properties of the transuranic lumiphore could be used in conjunction with laser systems.[13] Very recently, Roth et al.[14] used the UV absorption band to probe the two channels of $SOCl_2$ photodissociation via the resonance-enhanced multiphoton/time-of-flight (REMPI-TOF) technique, while Weiner and co-workers[15] probed the concerted versus stepwise $SOCl_2$ photodissociation using laser-induced fluorescence.

Other spectroscopic work includes several microwave studies that have led to determination of the hyperfine constants and the harmonic force field.[16] Besides the microwave region, gas-phase vibrational spectroscopy has been used to assign the six fundamental modes of pyramidal $SOCl_2$ using both Raman and infrared spectroscopy.[9,17−19] Infrared spectroscopy has also been used as a tool to investigate solvent effects on liquid-phase band positions and intensities.[20,21] Recently, both rapid-scan and step-scan time-resolved FTIR spectroscopy have been shown to be useful tools for investigating chemical kinetics.[22,23] DeVore and Gallaher[24] used time-resolved FTIR to investigate $SOCl_2$'s reaction with NO_2 in the gas phase and found that the initial reaction is first order in $SOCl_2$ and second order in NO_2, with the initial products being NOCl, NO_2Cl, and SO_2. Although $SOCl_2$ is known to react rapidly, even violently, with water in the condensed phase, relatively little is known about its *gas-phase* chemistry or general atmospheric fate, other than the reaction with NO_2. Since $SOCl_2$ is known to have a large vapor pressure (~100 Torr = 16 kPa at 298 K), we have chosen to investigate the hydrolysis of gas-phase $SOCl_2$ as a function of humidity under typical ambient conditions, as well as to verify its visible−ultraviolet absorption spectrum with regard to its atmospheric fate.

Experimental Methods

The present experiments were carried out in the Pacific Northwest National Laboratory (PNNL) wind tunnel. The wind tunnel can provide continuous circulation of air in a controlled environment by circulating the air through an enclosure shaped in a rectangular pattern approximately 15.5 m on the long sides and 3.5 m on the short sides. In the present experiments, however, a small portion of the tunnel, 0.61 × 0.61 m in cross-section and 1.85 m in length, was isolated and used to house

* Corresponding authors. E-mail: timothy.johnson@pnl.gov, crystal.driver@pnl.gov.

10.1021/jp022090v CCC: $25.00
Published on Web 07/22/2003

TABLE 1: Fitted Decay Constants and Hydrolysis Rates at Various Experimental Conditions

T (K)	P (mmHg)	RH (%)	H_2O concn (molecs/cm^3)	fitted decay constant k' (s^{-1})	hydrolysis rate (cm^3/molec-s)
296.2	743.0	3	2.04×10^{16}	9.30×10^{-4} [a]	3.82×10^{-20} [a]
296.2	748.2	3	2.04×10^{16}	4.49×10^{-4} [a]	1.72×10^{-20} [a]
297.2	748.2	3	2.16×10^{16}	3.57×10^{-4} [a]	1.52×10^{-20} [a]
299.2	746.1	3	2.42×10^{16}	6.13×10^{-4} [a]	8.48×10^{-21} [a]
297.2	746.1	4	2.88×10^{16}	5.34×10^{-4} [a]	4.75×10^{-21} [a]
295.2	739.1	6	3.86×10^{16}	3.19×10^{-4}	7.39×10^{-21}
296.2	743.0	7	4.77×10^{16}	5.92×10^{-4} [a]	1.81×10^{-20} [a]
298.2	743.0	7	5.34×10^{16}	2.84×10^{-4}	5.39×10^{-21}
297.2	743.0	10	7.21×10^{16}	6.49×10^{-4}	$(4.08 \pm 2.05) \times 10^{-21}$
297.2	743.0	11	7.93×10^{16}	5.88×10^{-4}	$(4.01 \pm 1.83) \times 10^{-21}$
297.2	739.1	12	8.65×10^{16}	5.72×10^{-4}	$(4.97 \pm 2.07) \times 10^{-21}$
296.2	749.7	18	1.23×10^{17}	8.21×10^{-4}	$(5.95 \pm 1.66) \times 10^{-21}$
296.2	749.7	19	1.29×10^{17}	6.92×10^{-4}	$(4.85 \pm 1.28) \times 10^{-21}$
297.2	739.1	28	2.02×10^{17}	1.95×10^{-3}	$(5.73 \pm 0.64) \times 10^{-21}$
297.2	743.0	35	2.52×10^{17}	1.21×10^{-3}	$(4.38 \pm 0.38) \times 10^{-21}$
297.2	740.8	35	2.52×10^{17}	1.12×10^{-3}	$(3.95 \pm 0.36) \times 10^{-21}$
297.2	748.2	47	3.39×10^{17}	1.42×10^{-3}	$(3.60 \pm 0.39) \times 10^{-21}$
296.2	748.2	49	3.34×10^{17}	1.99×10^{-3}	$(5.63 \pm 0.59) \times 10^{-21}$
297.2	748.2	49	3.53×10^{17}	1.71×10^{-3}	$(4.64 \pm 0.49) \times 10^{-21}$
297.2	740.8	73	5.26×10^{17}	6.73×10^{-3}	$(1.32 \pm 0.20) \times 10^{-20}$
297.2	740.8	74	5.34×10^{17}	8.18×10^{-3}	$(1.55 \pm 0.23) \times 10^{-20}$
296.2	748.2	85	5.79×10^{17}	1.05×10^{-2} [a]	$(1.80 \pm 0.54) \times 10^{-20}$ [a]
308.2	746.7	1	1.32×10^{16}	4.25×10^{-4} [a]	1.16×10^{-20} [a]
308.2	746.7	2	2.63×10^{16}	5.08×10^{-4} [a]	6.40×10^{-21} [a]
308.2	746.7	17	2.24×10^{17}	1.19×10^{-3}	$(4.03 \pm 1.19) \times 10^{-21}$
309.2	746.7	19	2.64×10^{17}	9.20×10^{-4}	$(2.96 \pm 0.78) \times 10^{-21}$
308.2	746.7	20	2.63×10^{17}	1.02×10^{-3}	$(3.38 \pm 0.54) \times 10^{-21}$
308.2	740.9	44	5.79×10^{17}	2.13×10^{-3}	$(3.53 \pm 0.25) \times 10^{-21}$
308.2	740.9	45	5.93×10^{17}	2.40×10^{-3}	$(3.96 \pm 0.29) \times 10^{-21}$
309.2	740.9	45	6.25×10^{17}	2.18×10^{-3}	$(3.35 \pm 0.23) \times 10^{-21}$
309.2	740.9	61	8.47×10^{17}	4.80×10^{-3}	$(6.78 \pm 0.65) \times 10^{-21}$
309.2	740.9	63	8.74×10^{17}	5.17×10^{-3}	$(6.34 \pm 0.52) \times 10^{-21}$

[a] Not used in fit.

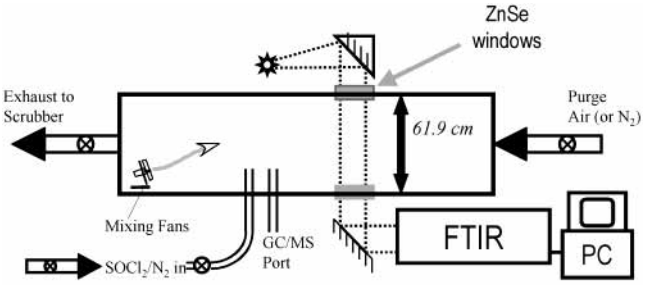

Figure 1. Experimental configuration for the $SOCl_2$ hydrolysis experiments. After purging of the system initially, the system is sealed off. At a certain time, the $SOCl_2$ is quickly added through a side port and mixed by the two chamber fans.

the molecular species of interest. Due to the corrosive nature of these species, the tunnel walls were lined and sealed with Teflon film in order to provide an inert surface, i.e., to minimize gas adsorption and heterogeneous chemistry on surfaces. Although the reaction vessel is essentially a "box", the large size of the chamber increases the volume/surface ratio, decreasing the importance of any wall reactions. The chamber was initially "conditioned" by allowing ~50 ppmv $SOCl_2$ to reside within the chamber for ~10 min prior to most experiments. The entire volume (690 L) was then purged and filled with room air adjusted to the desired temperature and humidity. After purging, the chamber was sealed, and an infrared reference spectrum (I_o) was recorded at atmospheric pressure ($739 < P < 750$ Torr, depending on the day and experiment). The hydrolysis experiment was begun and the parent compound released into the center of the chamber, as shown in Figure 1, where the entire mixture was continuously and vigorously stirred by two fans to achieve sample uniformity. To evaluate reproducibility, typically three experiments were carried out at each temperature and humidity. The reproducibility of the hydrolysis experiments was found to be good. The limiting factor, however, appeared to be the ability to prepare the large chamber with an atmosphere at exactly the same humidity and temperature. We estimate the uncertainties (2σ) in relative humidity to be 5% for RH <20%, 3% for 20−60% RH, and 10% for RH > 60%. The estimated temperature uncertainty is1 K; both parameters were measured using an Omega model RH-411 sensor. A total of 22 experiments were conducted at 297 ± 1.5 K, and 10 experiments at 309 K. Table 1 summarizes the temperatures and humidities of these experiments for both the 297 and 309 K data, as well as the (single-exponential) decay constants that were fit to the individual $SOCl_2$ decay curves. The sixth column also shows the calculated result for the hydrolysis rate coefficient (vide infra).

Due to its highly reactive and toxic nature, the $SOCl_2$ compound (Aldrich, 99% purity, CAS Registry No. 7719-09-7) was handled in a glovebox outside the chamber, where it was mixed with ultra-high-purity nitrogen carrier gas (>99.99%, Oxarc) and introduced to the wind tunnel chamber. All hardware in the delivery system was made of either stainless steel or Teflon. Also, because of the compound's highly toxic and reactive nature, the experiments were carried out using a pulsed-aliquot kinetic method (PAKM), whereby a single pulse (typically <40 s duration) of the $SOCl_2/N_2$ mixture was injected into the chamber at known temperature and humidity and mixed vigorously. This method allows safer handling of the compound, but the H_2O rate order must be extracted indirectly, as described below. These pulse durations lasted about 15−75 s, a relatively short time period compared to the compound decay times of

~2 to >60 min, depending on water concentration (vide infra). The inlet nozzle with the $SOCl_2/N_2$ mixture was approximately 20 cm from the probing IR beam, with the fans placed behind the inlet nozzle (see Figure 1). The mixing time under these conditions within the large chamber was tested in separate experiments with less reactive compounds and was found to be on the order of 10 s.

For the wind tunnel experiments, infrared spectroscopy proved to be the most useful technique, as it allowed us to simultaneously monitor both the parent compound ($SOCl_2$) and the formation products in a time-resolved fashion. A Midac model M2401-C emission FTIR was interfaced to the tunnel, as shown in Figure 1. The light from a glow bar infrared source on one side of the tunnel was collimated into a 38-mm-diameter beam. This IR beam was passed through the wind tunnel (using two AR-coated ZnSe windows) to the FTIR on the opposite side and reflected into the spectrometer's emission input port. (The single-pass distance, *d*, between the wind tunnel's ZnSe windows was measured to be 61.9 cm. In our analyses, we will assume the distribution of gas within the tunnel to be homogeneous.) The collimated infrared beam enters the classical Michelson interferometer and impinges upon a Ge/ZnSe beam splitter (600−6000 cm^{-1}) at a 45° angle of incidence in a classical Michelson-design interferometer that uses optical flats and a voice−coil drive mechanical scanner. The modulated beam was focused onto an MCT detector using a 38-mm-diameter 90°-off-axis paraboloid with a 38-mm focal length. The detector was a 77 K Infrared Associates (0.5 × 0.5 mm) mercury−cadmium−telluride detector, with a custom-installed 2.5-μm long-pass filter used to reduce the intensity for a more linear detector response. The MCT signal was increased with a preamplifier and then AC-coupled to a main amplifier board at unity gain, where it was sampled by a 16-bit 100 kilosample/s analog-to-digital converter to yield a sampling frequency $2\sigma v = 40$ kHz for the mirror moving at mechanical velocity v. Since the interferogram was sampled every half-wavelength of the HeNe laser, the spectral bandwidth of the measurement was that of the laser itself, namely $\sigma = 15\,798.0$ cm^{-1}. Single-sided, forward-scan interferograms were recorded at 4.0 cm^{-1} resolution. Raw interferograms were left in RAM memory; at the conclusion of the experiment, the interferograms were triangular-apodized, zero-filled an additional factor of 4, phase-corrected using the Mertz method,[25] and Fourier-transformed with the Cooley−Tukey algorithm. MidacGrams32 version 4.11 software was used to record the data, with further processing accomplished by WaveMetrics' IGOR Pro software, version 4.0.2.1. Other data parameters are standard for the Midac M2401-C and accord with the recommended reporting protocol for FTIR spectroscopic parameters.[26]

The IR reference spectra of SO_2, HCl, and other compounds analyzed herein were obtained from the PNNL Infrared Spectral Library.[27] In this database, each reference spectrum is derived from a fit to Beer's law constructed from 10 or more individual measurements at different burdens. The fit is constructed to represent exactly 1 ppmv-m at 25 °C. The noise level for the individual spectra is $<5 \times 10^{-4}$ OD, and the systematic error in intensity is <3% (2σ). Fortuitously, the spectrum of thionyl chloride has very significant IR structure in "the atmospheric window" between 700 and 1300 cm^{-1}. In particular, it has an especially strong band with a weak Q-branch centered at 1251 cm^{-1}. Because the Q-branch possessed too narrow a line width to be fully resolved with the current spectrometer, the system was set to 4 cm^{-1} resolution so as to be able to resolve the P and R branches of the strongest band. Data are presented directly in absorbance mode, $A = -\log(I/I_o)$. For the time evolution studies, the data are presented as 3D stacks (absorbance vs wavenumber vs time). Concentrations were derived using the Beer−Lambert absorption law, as discussed below. In these time-resolved studies, the number of interferogram co-additions was changed, depending on the relative humidity. Although the spectral resolution (4 cm^{-1}) was the same in all studies, for the high-humidity studies fewer interferograms were averaged in order to better capture the fast dynamics, whereas for the lower humidity measurements more co-additions were recorded for each individual "time-slice" spectrum in order to achieve better signal/noise ratios.

Chemical concentrations were also evaluated by gas chromatography−mass spectroscopy (GC−MS) using a Hewlett-Packard 5890 GC in conjunction with a Hewlett-Packard 5970 mass spectrometer. The GC column was a Restek Rtx 502.2, 30 m long, 0.32 mm i.d., with a 1.8-μm active layer. The data acquisition sequence used a 2-mL injection of air sample onto the column held at 100 °C. After 3 min, the temperature was ramped to 225 °C over a 10-min period. Thionyl chloride was found to elute at 3 min under these conditions. The air from the tunnel was sampled in 2-mL aliquots using a 5-cm^3 air-sampling syringe at the beginning, middle, and end of each IR data acquisition. Using standardized concentrations of $SOCl_2$ in dry air, the GC−MS system was found to have a linear response in the range from 5 to 100 ppmv.

In addition to the hydrolysis experiments conducted in the wind tunnel, ultraviolet/visible (UV/vis) spectra were recorded in a separate laboratory using a Shimadzu model 2501C dual-beam spectrometer with a 9.96-cm electrochemically polished gold-plated cell equipped with quartz windows. Data were recorded from 900 to 190 nm, with the slits set to 0.2 mm. The sample was freeze−pump−thawed four times to remove air. Initial experiments evidenced SO_2 as an impurity at approximately a 10% level. In subsequent experiments, the SO_2 was removed from the sample by pumping while maintaining the sample at ~220 K. UV/vis spectra were recorded only after verifying sample purity by infrared spectroscopy. Four different burdens of $SOCl_2$ were recorded, and the absorption coefficient was determined as the slope of a plot of absorbance versus concentration.[27] Our UV/vis data were found to be in good agreement with the results previously reported by Takacs and co-workers.[11]

Results

The results of a typical $SOCl_2$ hydrolysis experiment at high humidity (297 K, 74% RH) are displayed in Figure 2. A total of 32 such hydrolysis experiments were performed, but the product absorption signatures are more readily visible in a high-humidity experiment. The results are displayed as a stacked file with absorbance versus wavenumber versus time, where each "subfile" spectrum represents a time interval of 10.0 s (for this experiment). The infrared spectra reveal several features: First, the $SOCl_2$ band near 1251 cm^{-1} reaches a rapid maximum in about three time slices (30 s). At later times, the 1251 cm^{-1} band then shows a very distinct exponential decay, with a 1/*e* lifetime of 122 s. (The $SOCl_2$ decays were typically followed to longer times, but these time slices, as well as the time slices prior to introduction of the $SOCl_2$, have not been displayed in Figure 2.) Concomitant to the introduction of $SOCl_2$ and the rapid onset of its decay is the formation of SO_2(g), as evidenced by the growth of two bands, the strong ν_3 asymmetric stretch band near 1361 cm^{-1} as well as a weaker, broad doublet near 1151 cm^{-1} (ν_1 symmetric stretch).[28,29] Although the SO_2 ν_3 band

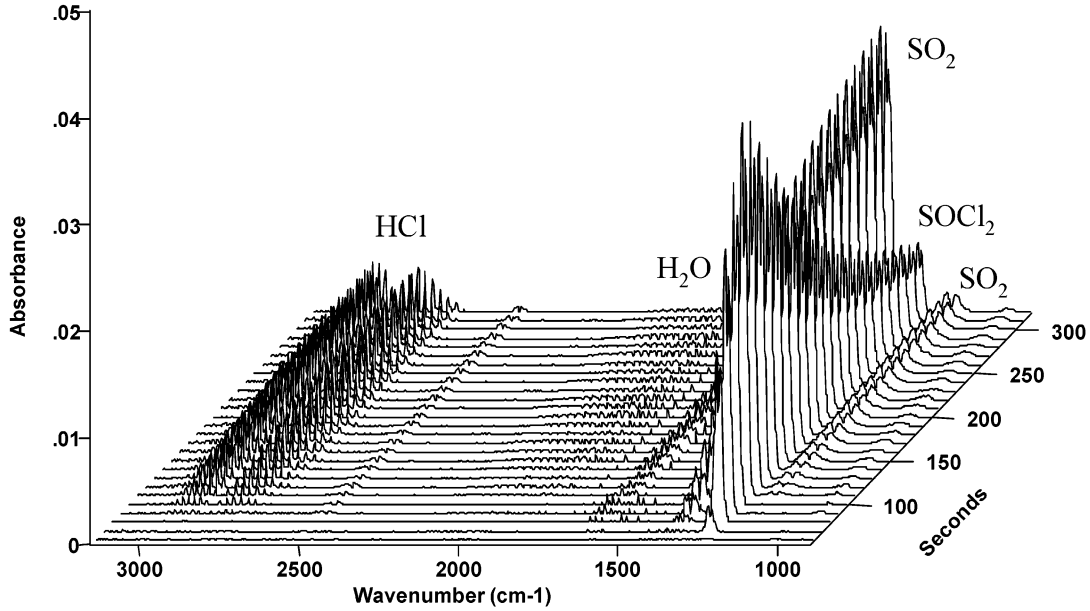

Figure 2. 3D dynamic infrared spectra of thionyl chloride hydrolysis during an experiment at 297 K and 74% relative humidity. The spectral resolution was 4 cm^{-1}, and the acquisition time for an individual spectrum (i.e., time between slices) is 10 s. Absorption bands due to specific molecules are labeled.

is the strongest band, it suffers from interferences by lines in the P branch of the water ν_2 bending mode, making quantitation somewhat difficult. In addition to formation of SO_2, the infrared spectra also show the formation of another product, namely the characteristic band of HCl gas centered at 2886 cm^{-1}. The HCl product is also first observed directly after introduction of the $SOCl_2$, and, similar to SO_2, it also follows a monotonically increasing growth curve. Of lesser importance, variations in the water and CO_2 concentrations are observed, as seen by the intensity changes in the water bending mode's rovibronic lines near 1604 cm^{-1} as well as in the ν_3 asymmetric stretch of CO_2 near 2350 cm^{-1}. The spurious water and carbon dioxide absorptions arise due to the two air spaces between the tunnel and source as well as between the tunnel and spectrometer, as seen in Figure 1. These spaces were not purged; the H_2O and CO_2 signals can therefore be ignored, as they arise from regions outside the chamber.

We note that, other than the HCl, SO_2, $SOCl_2$, H_2O, and CO_2 bands, no other species were identified in the infrared spectra. We also note that the concentrations observed with the GC−MS technique were in good agreement with those measured by IR. The only breakdown products observed by either GC−MS or infrared spectroscopy were SO_2 and HCl. With the exception of H_2, O_2, or Cl_2, infrared spectroscopy should in principle be able to identify all likely molecular formation products, provided there is sufficient sensitivity. For these kinetic studies, the molecular mixing ratios were derived by baseline-correcting the individual spectra using a multiple-point baseline fit. The data were then inspected for interferences and integrated over specific regions for each species. So long as Beer's law is obeyed, the integral is proportional to the molecular mixing ratio of each species, where the absorption coefficient [in $(ppmv\text{-}m)^{-1}$] is determined from the reference spectra.[27] For each spectrum, the corresponding mixing ratios were thus derived using the following wavenumber domains for analysis: HCl, 2884.6−2711.3 cm^{-1}; SO_2, 1397.2−1315.0 cm^{-1}; and $SOCl_2$, 1287.1−1215.9 cm^{-1}. For these experiments, the concentrations of $SOCl_2$, SO_2, and HCl were all derived from the same 3D plot of infrared spectra and are displayed versus time.

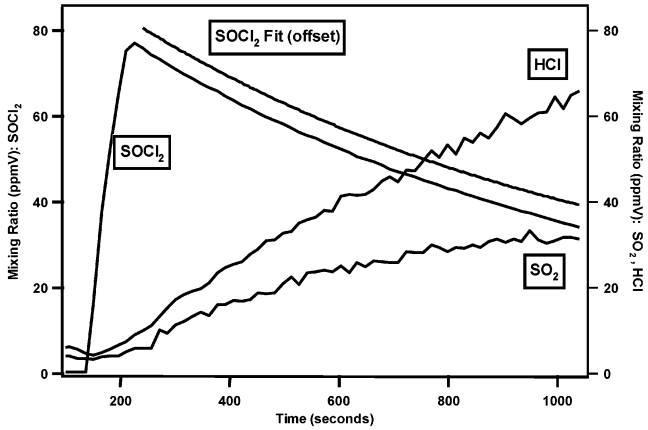

Figure 3. Rapid generation and decay curve of $SOCl_2$, along with the growth curves of the gaseous SO_2(g) and HCl(g) products in an experiment at 297 K and 35% RH. The acquisition time for an individual spectrum determines the grid spacing on the time axis and for this experiment was 15.1 s. Also displayed is a fit to $SOCl_2$ decay data; the theoretical curve is a single-exponential fit and has been offset for clarity.

Figure 3 presents typical integrated results, in this case for a 35% RH experiment at 297 K. Here the infrared data have been integrated to obtain mixing ratios (ppmv). Subsequently, all data were converted to concentrations using the appropriate temperatures/pressures. We see the thionyl chloride mixing ratio rising quickly from zero at $t = 135$ s to a maximum value near $t = 210$ s. After the $SOCl_2/N_2$ flow is switched off, the infrared spectra show that the $SOCl_2$ parent compound undergoes an exponential decay in concentration. A single-exponential curve was fit to this $SOCl_2$ decay and yielded the following values for this data set:

$$C_{SOCl_2} = 5.764 + 91.352 \exp(-0.001121t) \qquad (1)$$

where C_{SOCl_2} is the $SOCl_2$ mixing ratio in ppmv and the time t is measured in seconds. The $SOCl_2$ mixing ratio and the theoretical fit to the decay are plotted with the fit data vertically

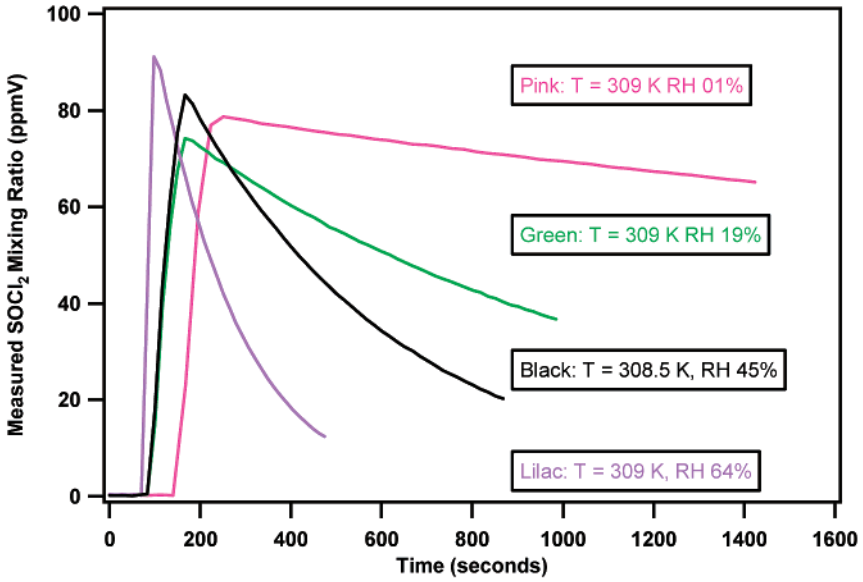

Figure 4. Multiple $SOCl_2$ decay curves as a function of relative humidity, all recorded from the ~309 K data set. Each curve was fit by a single-exponential decay (not shown). With no H_2O present in the chamber, the $SOCl_2$ decay rate was too long to be accurately measured with the present apparatus.

offset for clarity; the agreement is excellent. The same procedure was applied to each of the $SOCl_2$ decays, each yielding a different decay constant at the given humidity. Of the values in this equation, only the exponential constant $(1/\tau)$ is of significance, since the offset and pre-exponential terms are determined by when the $SOCl_2$ is introduced and its initial concentration, both of which are easily varied and hence arbitrary parameters. If reproducible, the exponential decay constant should depend only on the temperature and relative humidity (vide infra). To test this, the experiment was carried out a total of three times at the same nominal temperature and humidity to determine the reproducibility of the τ constant. For example, for the three experiments at 309 $\pm$ 1 K and RH 18.0 $\pm$ 1.5%, the decay constant was found to be $(1/\tau) = 0.00104 \pm 0.00013$. The parameter τ will be shown below to contain information about the hydrolysis rate coefficient. We note again that the greatest source of experimental error was the difficulty in preparing and measuring an air mass this large at a constant temperature and relative humidity. The problem was exacerbated by the fact that, at high humidity, the $SOCl_2$ was observed to corrode the temperature/humidity sensor. Nevertheless, for our 32 experiments ranging from 1 to 85% humidity, $SOCl_2$ decay showed single-exponential decay behavior.

Figure 3 also displays the formation curves for both SO_2(g) and HCl(g), which were obtained from the infrared spectra in the same fashion. The formation of these two products occurs within the first time interval after addition of the $SOCl_2$, indicating a rapid onset of reaction. There is also some evidence of SO_2 and HCl, especially HCl, near times $t = 0$ (i.e., before the $SOCl_2$ has been introduced). This is in part due to the spectrometer baseline drift and the fact that the software measures all values above the baseline (including noise). In the case of HCl, however, another small effect manifested itself: *After* the $SOCl_2$ reactant was mostly or completely depleted, the SO_2 values remained nearly constant, but the gas-phase HCl absorptions showed slight decreases with additional lapse of time. Since the chamber was sealed, we ascribe this to small amounts of HCl adsorbing to the walls and/or components inside the chamber. It was further observed that, after the chamber was purged with fresh air, very small concentrations of gas-phase HCl were seen to slowly build up, lending further credence to a sorption/desorption hypothesis. The adsorption effect took place predominantly after the experiments were complete, as HCl is known to be a very polar molecule that readily adsorbs to surfaces, even Teflon, with long-lasting memory effects.[30,31] The ppb-level effect was minimized here by working at ppm-level concentrations, and also recognizing that the HCl is a product, not a reactant.

The small HCl adsorption effect notwithstanding, upon hydrolysis of the $SOCl_2$, *gaseous* HCl and SO_2 were formed simultaneously in a stoichiometric ratio of approximately 2:1, as shown in Figure 3. This relationship was observed in each of the 32 experiments performed. The stoichiometry was averaged over 20 of the experiments (excluding experiments with insignificant HCl and SO_2 production) and was determined to be 1.66 ± 0.45. A 2:1 stoichiometry for HCl:SO_2 production is thus shown within the experimental uncertainty. We observe that the calculated values for the SO_2 and HCl mixing ratios have larger uncertainties than those of $SOCl_2$ due to their smaller absorption coefficients compared to $SOCl_2$, as well as their greater susceptibility to water interferences. It is important to note that gaseous SO_2 and HCl were the only products identified in the FTIR spectra. The GC−MS data also showed HCl(g) and SO_2(g) as the only appreciable products.

Figure 4 juxtaposes the degradation of $SOCl_2$ at four different humidities. All these data were recorded at 309 $\pm$ 1 K, and each trace corresponds to a single experiment at a different humidity. As seen in the figure, the decay time for thionyl chloride decreases rapidly with increasing humidity. The observation that the $SOCl_2$ curves do not all rise at the same time is due to the sample injection time variability among experiments. Aliquots of approximately equal concentrations of $SOCl_2$ were achieved by using pulses of similar duration. For the very high humidity experiments, the aliquot duration was increased somewhat due to the rapid consumption of the reactant during the initial stages of reaction. In addition to a faster decay, the high-humidity traces make more evident the exponential nature of the $SOCl_2$ decay. Figure 4 also shows a very low humidity decay curve (RH 01%), where the $d[SOCl_2]/dt$ decay is seen to be very slow, with a half-life on the order of several hours. In addition to the curves displayed in Figure 4, an experiment was carried out (not shown) where the tunnel

was purged of all water down to the < tens of ppm level. As expected, with little or no water, $d[SOCl_2]/dt \approx 0$, to within the noise level of the spectrometer.

For the UV/vis data, our results were found to agree with those of Takacs et al.[11] Thionyl chloride exhibits no absorbance in the range from 300 to 900 nm (i.e., a colorless species). The $SOCl_2$ spectrum exhibits two very strong bands in the ultraviolet, with absorption maxima at $\lambda = 247$ nm (40 500 cm^{-1}) and $\lambda <$ 200 nm. The lack of significant absorption at wavelengths longer than 290 nm, however, is the observation of greater significance for the atmospheric fate of this species, because it shows tropospheric photolysis to be of lesser importance.

Data Analysis and Discussion

The $SOCl_2$ temporal plots, exemplified by Figure 4, illustrate an additional important feature, namely that the time scale for $SOCl_2$ concentration rise is much shorter than the decay time. This allows the decay of $SOCl_2$ to be treated independently of the initial increase in $SOCl_2$ concentration. Thus, only two reactions will be assumed important in describing the decay of $SOCl_2$ in each experiment and are given as

$$SOCl_2 + H_2O \rightarrow 2HCl + SO_2 \quad (2)$$

$$SOCl_2 \rightarrow \text{products} \quad (3)$$

where reaction 2 is the homogeneous hydrolysis described by a rate coefficient k_h, and reaction 3 is a first-order loss process used to characterize both the reactive and nonreactive uptake of $SOCl_2$ onto the internal surfaces (e.g., walls) described by k_w.

The general rate equation for the $SOCl_2$ hydrolysis is given by

$$d[SOCl_2]/dt = -k_h[SOCl_2]^a[H_2O]^b \quad (4)$$

For these experiments, clearly $[H_2O] \gg [SOCl_2]$, and we can rewrite the rate equation

$$d[SOCl_2]/dt = -k'[SOCl_2]^a \quad (5)$$

where

$$k' = k_h[H_2O]^b \quad (6)$$

If the reaction is first-order in $SOCl_2$, then $a = 1$ and $\ln[SOCl_2(t)/SOCl_2|_{t=0}] = -k't$; hence, we should observe a pseudo-exponential decay.[32] For each of the 32 hydrolysis experiments, a single-exponential decay curve was fit to the measured data. For most of the experiments, the decay curve was followed over one to two 1/*e* lifetimes. The exceptions to this were when the spectrometer noise level prevented obtaining accurate concentrations (for low $SOCl_2$ concentrations), or for the very low humidity experiments, e.g., 3% RH, where the decay time for an individual experiment would correspond to a significant fraction of a day. An example of one of the observed exponential decays, along with the fit to a single-exponential term (showing the reaction to be first order in $SOCl_2$), is shown in Figure 3. The raw data from four additional $SOCl_2$ decays at 309 K (showing the effect of RH) are presented in Figure 4. Although the fits are not displayed in Figure 4, essentially all of the $SOCl_2$ decay curves was fit very well by a single-exponential decay, thus showing $a = 1$.

The order with respect to water is also clearly of interest. Since we have not one but many hydrolysis experiments, we can use the inverse of the decay lifetime $(1/\tau') = k'$ from each of the $SOCl_2$ decay curves and take the logarithm of eq 6 to obtain

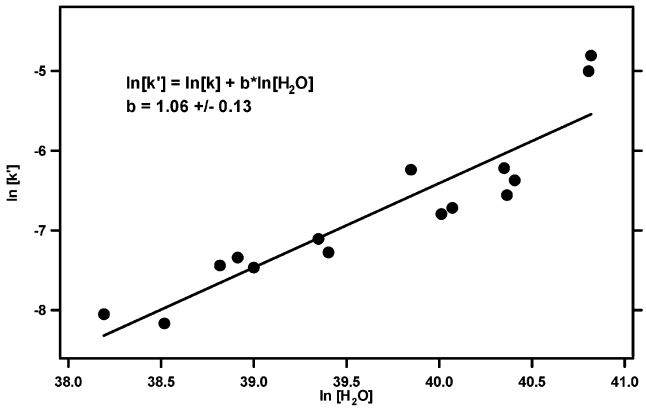

Figure 5. Plot of $\ln(k')$ versus $\ln [H_2O]$ for the series of multiple hydrolysis experiments at 297 K, each at a different humidity. k' $(=1/\tau_{obs})$ is the pseudo-first-order rate constant for $SOCl_2$ where water is in excess. The slope b is the reaction order with respect to water.

$$\ln(k') = \ln(k_h) + b \ln [H_2O] \quad (7)$$

Thus, if we use an entire set of decay curves such as those in Figure 4, each at a known humidity and measured exponential decay constant k', a plot of $\ln(k')$ versus $\ln [H_2O]$ yields as slope the reaction order with respect to water, b. Figure 5 plots $\ln(k')$ versus $\ln [H_2O]$ for the 297 K experiments, and as can be seen from the plot, the agreement is good. In making this 297 K fit, one datum was excluded at very high humidity (85%) due to visible (water) condensation in the chamber; presumably, the outer walls were slightly cooler, leading to condensation with time at high RH. We have also discarded most points at low humidity (<7%). The reasons for discarding these low RH data are two-fold. First, concerning the *x*-values, the humidity sensor is quite unreliable at the low humidities and the fractional error grows very rapidly, for example, depending on whether the sensor displays either 2 or 3% RH. Second, concerning the *y*-values, at the low humidities, the $SOCl_2$ hydrolysis can have a half-life of several hours or more (e.g., Figure 4), and as a consequence, the data do not follow the decay over even a single 1/*e* lifetime, yielding less-reliable single-exponential fits. Nevertheless, in Figure 5, the slope of the fit was determined to be $b = 1.06 \pm 0.13$, meaning that, to within experimental error, the reaction is first order in water, i.e., $b = 1$.

If we now take both $a = b = 1$, the rate constant k_h for the overall hydrolysis rate expression (eq 4) can be obtained directly from any of the independent hydrolysis experiments by substituting the measured concentrations and reaction rate. For our data, the mixing ratios (in ppmv) had to first be converted to concentrations (molecules/cm^3) using the wind tunnel temperature and pressure for the given day/experiment. Using the fitted decay curves to determine the slope $d[SOCl_2]/dt$, the overall rate constant k_h was determined for each experiment by using eq 4 with both *a* and *b* taken as 1. The individual values obtained using this method are displayed as column 6 in Table 1. For the 297 K data, we determined an average value of $k_{h(297)} = (6.3 \pm 3.5) \times 10^{-21}$ cm^3/(molecule-s), which represents an average of 15 experimental decays, where we have intentionally discarded the experiments at low humidities and the one very high humidity datum for the reasons described above. For the 309 K data, k_h was determined to be $k_{h(309)} = (4.3 \pm 1.5) \times 10^{-21}$ cm^3/(molecule-s), as derived from eight measurements.

These 10^{-21} cm^3/(molecule-s) values represent a somewhat slow reaction but are plausible for a bimolecular rate coefficient for these close-shelled species.[33] Since there are only two temperature points and the uncertainties in the determined rate constants are large, conjecture about Arrhenius activation energies is not warranted. Clearly, a wide range of temperatures needs to be studied to discuss activation energies, but the present system does not accommodate these experiments.

Our analysis has suggested, but does not prove, that the $SOCl_2$ hydrolysis *may* occur as part of an elementary reaction, perhaps as a single reactive complex. The observed pseudo-first-order behavior seen for all the decay curves (with water in excess) shows the hydrolysis reaction 2 to be first order in $SOCl_2$. The dependence on water was investigated by first observing that $d[SOCl_2(g)]/dt \approx 0$ in the absence of water (see, e.g., the RH 01% upper trace in Figure 4); the rate order in $[H_2O]$ was then determined (with less confidence than the rate order for $SOCl_2$) by using the decay constants from the hydrolysis at several different humidities to yield $b = 1$. In the absence of further temperature and pressure studies, it is difficult to draw absolute conclusions as to the mechanism; our data are consistent with a gas-phase hydrolysis but do not preclude a heterogeneous or aerosol-catalyzed degradation.

The corroborative evidence to support a homogeneous hydrolysis mechanism includes the absence of aerosols in the synthetic atmosphere within the chamber. Also consistent with the mechanism of eq 2 is that the two products HCl(g) and SO_2(g) were both formed as gases, that they were formed in 2:1 stoichiometric amounts (HCl to SO_2), and that they were also the only products observed by either the IR or GC−MS technique. Further, the mixing time for the system was on the order of 10 s, and Figure 2, for example, shows formation of both gas-phase HCl and SO_2 within 20 s, making it fortuitous that the $SOCl_2$ could be mixed to the walls, heterogeneously hydrolyzed, and then have the gaseous products diffuse back into the IR beam. This certainly does not *preclude* a surface-catalyzed reaction between H_2O and $SOCl_2$, but the IR spectra showed both the SO_2 and HCl products directly in the gas phase. However, if the SO_2(g) and HCl(g) are direct products of the proposed hydrolysis reaction 2, then not only should their stoichiometry be 2:1 (as was observed within experimental error), but their formation rates should match the decay rate of $SOCl_2$. This was indeed the case. If, in a given experiment, e.g., 25 ppmv of $SOCl_2$(g) was consumed over a certain time, ~25 ppmv of SO_2(g) was formed. For the gas-phase HCl, the agreement between 2 HCl formed for each 1 $SOCl_2$(g) consumed was not quite as good. The ratio was typically <2 for HCl, presumably due to HCl's weak IR signal and the HCl adsorption phenomenon discussed above.

Thus, although we cannot rule out the possibility of heterogeneous chemistry giving rise to the observed hydrolysis, we observed pseudo-first-order decay in $SOCl_2$ for all experiments, combined with the stoichiometric formation of 1 SO_2(g) and 2 HCl(g), which is consistent with reaction 2. Should some heterogeneous process be responsible for the mechanism, it is also fortuitous that the reaction rate increases proportional to the humidity. Nevertheless, in the absence of further experiments, it is difficult to conclusively assign the reaction as homogeneous bimolecular, since the misassignment of reaction orders and mechanisms has occurred before. In a seemingly analogous reaction between SO_3 and water vapor, recent work by Kolb and co-workers[34,35] and Lovejoy and co-workers[36] established that the SO_3 reaction is, in fact, second order in water vapor, though originally thought to be first order. Our data do not indicate this for the $SOCl_2$ hydrolysis, as the slope in Figure 5 is quite close to 1. Clearly, more temperatures must be studied to determine an activation energy, and it would be well to try other techniques to further investigate the $SOCl_2$ hydrolysis, such as the turbulent flow/CIMS technique used by Kolb et al.,[35] or possibly using isotopically labeled species. Matrix isolation techniques have proven useful at isolating such intermediates,[37] and recently step-scan FTIR has proven useful at elucidating intermediates for reactions that can be triggered in a reproducible manner.[38,39] Further temperature and pressure studies are warranted but are not feasible in the present configuration.

For typical boundary layer conditions of $T = 298$ K and 50% relative humidity, the 6.3×10^{-21} cm^3/molecule-s rate constant corresponds to a 1/*e* lifetime of 423 s (7.0 min). Another conceivable loss process in the atmosphere could be reaction with the hydroxyl radical OH. Assuming gas-kinetic-limited reaction conditions of $k \approx 3 \times 10^{-12}$ cm^3/molecule-s and a typical midlatitude daytime tropospheric OH concentration[40] of 5×10^6 molecules/cm^3, one obtains a tropospheric lifetime of 18.5 h. These considerations reveal that hydrolysis, and not photolysis or reaction with OH, will be the dominant degradation pathway for $SOCl_2$ under typical boundary layer conditions. It should be noted that partial motivation for this work is to develop a database of hydrolysis rate coefficients for inorganic species so as to enable structure−activity relationships for inorganic compounds to be developed to the extent that they are for the oxidation of organic compounds.

Summary

The atmospheric fate of $SOCl_2$ has been investigated in a sealed mixing chamber by simulating the effects of varied temperature and humidity. It was determined that humidity plays an important role, as water reacts rapidly with the parent compound, forming HCl(g) and SO_2(g) in a nearly stoichiometric ratio of 2:1. The rate constant for hydrolysis at 297 K was determined to be $k_h = (6.3 \pm 3.5) \times 10^{-21}$ cm^3/molecule-s, resulting in a tropospheric lifetime due to hydrolysis on the order of only a few minutes for this volatile inorganic species. To the best of our knowledge, this is the first reported kinetic study on the gas-phase hydrolysis of $SOCl_2$.

Acknowledgment. The authors thank Dr. Steven Sharpe of the Pacific Northwest National Laboratory for a review of the manuscript. We are also grateful to the reviewers of this manuscript for many helpful suggestions. This work was performed at the PNNL wind tunnel facility. PNNL is operated for the U.S. Department of Energy by the Battelle Memorial Institute under Contract DE-AC06-76RLO 1830.

References and Notes

(1) Corio, L. A.; Ziolkowski, T. S.; Walker, J. K.; Jones, W. B.; Belisle, T. Assessment of the Impact of Exhausted Toxic Emissions on Indoor Air Quality at the Naval Air Weapons Station at China Lake, California. *Proc. Annu. Meet. Air Waste Mgmt. Assoc.* **1996**, *89*, wp8503/1−wp8503/16.

(2) See, for example: (a) Creary, X.; Tricker, J. Reaction of Benzylic α-Hydroxythioamides with Thionyl Chloride. *J. Org. Chem.* **1998**, *63*, 4907−4911. (b) Pizzey, J. S. *Synthetic Reagents*; John Wiley & Sons: New York, 1974; Vol. 1, pp 321−357.

(3) Lang, S. J.; Morrow, B. A. Infrared Spectra of Chlorinated Silica. *J. Phys. Chem.* **1994**, *98*, 13314−13318.

(4) Levy, S. C. Safety and Reliability Studies of Primary Lithium Batteries. *J. Power Sources* **1993**, *43*, 347−351.

(5) Wagner, C. G. Lithium/Sulfur Dioxide Cells and Lithium/Thionyl Chloride Cells—Safe Use and Testing. *Proc. Int. Power Sources Symp.* **1992**, *35*, 125−128.

(6) Venkatasetty, H. V. Cyclic Voltammetric and Spectroscopic Studies of $SOCl_2$ Solutions. *J. Electrochem. Soc.* **1980**, *127*, 2531−2533.

(7) Kim, B.-S.; Park, S.-M. Spectroelectrochemical Studies on the Reduction of Thionyl Chloride. *J. Electrochem. Soc.* **1995**, *142*, 34−40.

(8) Kim, B.-S.; Park, S.-M. Aggregation of Thionyl Chloride in Organic Solvents. *J. Phys. Chem.* **1995**, *99*, 9918−9923.

(9) Mosier-Boss, P. A.; Boss, R. D.; Gabriel, C. J.; Szpak, S.; Smith, J. J.; Nowak, R. J. Raman and Infrared Spectroscopy of the $AlCl_3$−$SOCl_2$ System. *J. Chem. Soc., Faraday Trans. 1* **1989**, *85*, 11−21.

(10) Asundi, R. K.; Samuel, R. Absorption Spectra of the Chlorides and Oxychlorides of Sulphur. *Proc. Phys. Soc. London* **1936**, *48*, 28−34.

(11) Uthman, A. P.; Demlein, P. J.; Allston, T. D.; Withiam, M. C.; McClements, M. J.; Takacs, G. A. Photoabsorption Spectra of Gaseous Methyl Bromide, Ethylene Dibromide, Nitrosyl Bromide, Thionyl Chloride, and Sulfuryl Chloride. *J. Phys. Chem.* **1978**, *82*, 2252−2257.

(12) Abraham, K. M.; Alamgir, M. Spectroscopic and Electrochemical Studies on Some Halogens and Interhalogens in $SOCl_2$. *J. Electrochem. Soc.* **1987**, *134*, 2112−2118.

(13) Batyaev I. M.; Kabatskii, Y. A.; Soklakova N. A. Luminescent-Spectral Properties of the $SOCl_2$−$GaCl_3$ System Activated by Uranyl. *Radiochem* **1993**, *35* (2), 176−178.

(14) Roth, M.; Maul, C.; Gericke, K.-H. Competitive Channels in the Photodissociation of Thionyl Chloride. *Phys. Chem. Chem. Phys.* **2002**, *4*, 2932−2940.

(15) Wang, H.; Chen, X.; Weiner, B. R. Laser Photodissociation Dynamics of Thionyl Chloride: Concerted and Stepwise Cleavage of S−Cl Bonds. *J. Phys. Chem.* **1993**, *97*, 12260−12268.

(16) Müller, H. S. P.; Gerry, M. C. L. Microwave Spectroscopic Investigation of Thionyl Chloride, $SOCl_2$: Hyperfine Constants and Harmonic Force Field. *J. Chem. Soc., Faraday Trans.* **1994**, *90*, 3473−3481 and references therein.

(17) Martz, D. E.; Lagemann, R. T. Infrared Spectra of Thionyl Chloride and Sulfuryl Chloride. *J. Chem. Phys.* **1954**, *22*, 1193−1195.

(18) Suthers, R. A.; Henshall, T. A Vibrational Analysis of the Thionyl and Seleninyl Halides. *Z. Anorg. Allg. Chem.* **1972**, *388*, 269−276.

(19) Hopf, G.; Paetzold, R. Untersuchungen an Selen-Verbindungen. *Z. Phys. Chem.−Leipzig.* **1972**, *251*, 273−279.

(20) David J. G.; Hallam, H. E. Solvent Effects on Infrared Band Shapes and Intensities Part 3. Band Contours of ν_1 and ν_2 of SO_2 and ν_1 of $SOCl_2$. *J. Mol. Struct.* **1970**, *5*, 31−36.

(21) Nanni, P.; Viani, F. Solvent Effects on the Infrared Spectra of Thionyl and Seleninyl Chlorides. *J. Mol. Struct.* **1972**, *14*, 413−419.

(22) Johnson, T. J.; Simon, A.; Weil, J. M.; Harris, G. W. Applications of Time-resolved Step-Scan and Rapid-Scan FT-IR Spectroscopy: Dynamics from Ten Seconds to Ten Nanoseconds. *Appl. Spectrosc.* **1993**, *47*, 1376−1381.

(23) Strong, K.; Johnson, T. J.; Harris, G. W. Visible Intracavity Laser Spectroscopy with a Step-scan Fourier Transform Interferometer. *Appl. Opt.* **1997**, *36*, 8533−8540.

(24) DeVore, T. C.; Gallaher, T. N. Infrared Spectroscopic Investigation of the Reaction between $SOCl_2$ and NO_2. *Inorg. Chem.* **1984**, *23*, 3506−3509.

(25) Mertz, L. Auxiliary Computation for Fourier Spectrometry. *Infrared Phys.* **1967**, *7*, 17−23.

(26) Bertie, J. E.; et al. Specification of Components, Methods and Parameters in Fourier Transform Spectroscopy by Michelson and Related Interferometers. *Pure Appl. Chem.* **1998**, *70* (10), 2039−2045.

(27) Sharpe, S. W.; Sams, R. L.; Johnson, T. J.; Chu, P. M.; Rhoderick, G. C.; Guenther, F. R. Creation of 0.10 cm^{-1} Resolution, Quantitative, Infrared Spectral Libraries for Gas Samples. In *Vibrational Spectroscopy-based Sensor Systems*; Christesen, S. D., Sedlacek, A. J., III, Eds.; Proceedings of SPIE 4577; SPIE: Bellingham, WA, 2002; pp 12−24. (b) http://nwir.pnl.gov.

(28) Herzberg, G. *Molecular Spectra and Molecular Structure, II. Infrared and Raman Spectra of Polyatomic Molecules*; Van Nostrand Reinhold Co.: New York, 1945.

(29) Sumpf, B. Line Intensity and Self-broadening Investigations in the ν_1 and ν_3 bands of SO_2. *J. Mol. Struct.* **2001**, *599*, 39−49.

(30) Freid, A.; Sams, R.; Berg, W. W. Application of Tunable Diode Laser Absorption for Trace Stratospheric Measurements of HCl: Laboratory Results. *Appl. Opt.* **1984**, *23* (11), 1867−1880.

(31) Harris, G. W.; Klemp, D.; Zenker, T. An Upper Limit on the HCl Near-Surface Mixing Ratio over the Atlantic Measured Using TDLAS. *J. Atmos. Chem.* **1992**, *15*, 327−332.

(32) Levine, I. N. *Physical Chemistry*, 2nd ed.; McGraw-Hill: New York, 1983; Chapter 17.

(33) Seinfeld, J. H.; Pandis, S. N. *Atmospheric Chemistry and Physics: From Air Pollution to Climate Change*; John Wiley & Sons: New York, 1998.

(34) Kolb, C. E.; Jayne, J. T.; Worsnop, D. R.; Molina, M. J.; Meads, R. F.; Viggiano, A. A. Gas-Phase Reaction of Sulfur Trioxide with Water Vapor. *J. Am. Chem. Soc.* **1994**, *116*, 10314−10315.

(35) Jayne, J. T.; Pöschl, U.; Chen, Y.-M.; Dai, D.; Molina, L. T.; Worsnop, D. R.; Kolb, C. E.; Molina, M. J. Pressure and Temperature Dependence of the Gas-Phase Reaction of SO_3 with H_2O and the Heterogeneous Reaction of SO_3 with H_2O/H_2SO_4 Surfaces. *J. Phys. Chem. A* **1997**, *101*, 10000−10011.

(36) Lovejoy, E. R.; Hanson, D. R.; Huey, L. G. Kinetics and Products of the Gas-Phase Reaction of SO_3 with Water. *J. Phys. Chem.* **1996**, *100*, 19911−19916.

(37) Tso, T.-L.; Lee, E. K. C. Formation of Sulfuric Acid and Sulfur Trioxide/Water Complex from Photooxidation of Hydrogen Sulfide in Solid O_2 at 15 K. *J. Phys. Chem.* **1984**, *88*, 2776−2781.

(38) Letendre, L. T.; Dai, H.-L.; McLaren, I. A.; Johnson, T. J. Interfacing a Transient Digitizer to a Step-scan Fourier Transform Spectrometer for Nanosecond Time-resolved Spectroscopy. *Rev. Sci. Instrum.* **1999**, *70*, 18−22.

(39) Dattelbaum, D. M.; Hartshorn, C. M.; Meyer, T. J.; Direct Measurement of Excited-state Intervalence Transfer in $[(tpy)Ru^{III}(tppz^{\bullet-})Ru^{II}(tpy)]^{4+*}$ by Time-resolved Near-infrared Spectroscopy. *J. Am. Chem. Soc.* **2002**, *124*, 4938−4939.

(40) Finlayson-Pitts, B. J.; Pitts, J. N., Jr. *Chemistry of the Upper and Lower Atmosphere*; Academic Press: New York, 1999.